A weighted-RV method to detect fine-scale functional connectivity during resting state

Hui Zhang [a], Xiaopeng Zhang [a], Yingshi Sun [a], Jiangang Liu [d], Wu Li [b], Jie Tian [b,c],*

[a] Key Laboratory of Carcinogenesis and Translational Research (Ministry of Education), The Department of Radiology, Peking University Cancer Hospital & Institute, China
[b] Institute of Automation, Chinese Academy of Science, Beijing 100190, China
[c] Life Science Research Center, Xidian University, Xi'an, Shaanxi 710071, China
[d] School of Computer and Information Technology, Beijing Jiaotong University, Beijing 100044, China

ARTICLE INFO

ABSTRACT

During the resting state, in the absence of external stimuli or goal-directed mental tasks, some functionally related discrete regions of the brain show complex low-frequency fluctuations in the blood oxygenation level dependent signal. Here we developed a novel ROI-based multivariate statistical framework to obtain the fine-grained patterns of functionally specialized brain networks in the resting state. Under this framework, the weighted-RV method is proposed and used to detect the spatial fine-scale patterns of functional connectivity. This approach overcomes several major problems of the traditional resting-state data analysis methods such as Pearson correlation and linear regression analysis. By using simulation and real fMRI experiment, we have found that the weighted-RV method is shown to be more sensitive in detecting the fine-scale based low-frequency connectivity even at a very low functional contrast-to-noise ratio (CNR), and this method can achieve much better performance in mapping the fine-grained patterns of functionally specialized brain networks compared to the traditional methods.

© 2010 Elsevier Inc. All rights reserved.

Introduction

Recent studies have found that, in the absence of external stimuli or goal-directed mental tasks, several functionally related discrete regions of brain show spontaneously synchronized low-frequency fluctuations in the blood oxygenation level dependent signal. These synchronized fluctuations suggest the existence of complex functional connectivity between these discrete local regions and fine-grained patterns of functionally specialized brain network in resting state (Biswal et al., 1995; Lowe et al., 1998; Xiong et al., 1999; Greicius et al., 2003; Fox et al., 2005; Beckmann et al., 2005; Nir et al., 2006; Achard et al., 2006; Damoiseaux et al., 2006). By using region of interest (ROI)-based analysis method, a set of functionally specialized resting-state networks (RSN) have been identified, such as the motor network (Biswal et al., 1995; Lowe et al., 1998; Xiong et al., 1999), the visual network (Lowe et al., 1998), the language network (Hampson et al., 2002), the default network (Greicius et al., 2003), and the anti-correlated functional networks (Fox et al., 2005).

Traditional ROI-based methods measure the correlation between the BOLD time course from a seed region and the time course from all other voxels in the brain. The measure of the correlation is based on Pearson correlation coefficient (Fox et al., 2005) or the linear regression parameter (Greicius et al., 2003). These analysis methods are widely used owing to their sensitivity, simplicity, and ease of interpretation. However, they also have some problems. To gain better insight into the resting neural network, it is important to investigate the connectivity information of the functional brain regions at multiple spatial scales, especially at fine scale (Margulies et al., 2007; Cohen et al., 2008). The fine-scale information allows for understanding the functional-connectivity information in a highly localized fashion. The traditional ROI-based correlation analysis such as Pearson correlation and linear regression analysis are based on voxel-by-voxel calculation. Since the functional brain regions are usually clustered together and regionally rendered homogeneous (Zang et al., 2004), such fine spatial structure information is lost during this univariate analysis process. In addition, for a variety of reasons, fMRI data contain a large amount of spatial random noise, and univariate analysis method is highly susceptible to the noise. This leads to a salt-and-pepper-like connectivity map when using conventional methods, such as Pearson correlation and linear regression. In order to suppress the spatial noise, the fMRI volumes are often smoothed before performing the correlation analysis. However, as a consequence, this strategy also makes the connectivity map blurred and obscure or even loses the fine-grained functional connectivities between different nearby regions.

How to find a win–win strategy to extract the fine-grained structure of the connectivity patterns as well as to suppress the spatial random noise? In this study, we aimed to improve the ROI-based method by proposing a multivariate statistical framework for analyzing the functional

* Corresponding author. Medical Image Processing Group, Key Laboratory of Complex Systems and Intelligence Science, Institute of Automation Chinese Academy of Science, Graduate School of the Chinese Academy of Science, P.O. Box 2728, Beijing 100190, China. Fax: +86 10 62527995.
E-mail addresses: tian@ieee.org, jie.tian@ia.ac.cn (J. Tian).
URL's: http://www.mitk.net, http://www.3dmed.net (J. Tian).

connectivity of the brain network during the resting state. Within this framework, the multivariate statistic of RV coefficient is employed. The RV coefficient was firstly introduced by Robert and Escoufier (1976) (Escoufier, 1973). This multivariate statistic provides a very efficient way to measure the similarity between two sets of variables with the same number of sample observations (Abdi, 2007). In the present study, we use RV coefficient to measure the spatial connectivity patterns between the region of interest and each local region of the whole brain. For suppressing the spatial noise while keeping the spatial features, we generate an adaptive anisotropic weight template, borrowing the idea of bilateral filtering in imaging processing (Tomasi and Manduchi, 1998). The weight template is then added to the multivariate framework. The advantage of using this multivariate method is that the connectivity calculation is more consistent with the hypothesis that the function-homogeneous voxels of brain volume are spatially clustered within a local region (Zang et al., 2004). Similar strategies have ever been proposed and have been used in detecting brain activity. For example, Friman et al. (2003) used a steerable filter and the multivariate statistical model of canonical correlation analysis (CCA) to adaptively detect local activity patterns. Kriegeskorte et al. (2006) used a searchlight and multivariate statistic of Mahalanobis distance to detect the response patterns within each local region. While in the present study, we focus on the fine-scale pattern of connectivity analysis.

In this study, we used simulation and real fMRI data to explore whether our multivariate statistical framework with weighted-RV statistic can be used to maintain fine-scale spatial functional-connectivity information and at the same time reduce the influence of spatial random noise. We aimed to ascertain whether our method is particularly more sensitive than the traditional ROI-based univariate method in detecting the fine-scale patterns of low-frequency resting-state connectivity at very low functional contrast-to-noise ratio (CNR).

Methods

The multivariate framework for the analysis of functional connectivity

To investigate the intensity of functional connectivity of each brain location with a particular region of interest (ROI), a continuous functional-connectivity map is needed. Similar to the "searchlight" used by Kriegeskorte et al. (2006), we obtain a search cube centered on a particular voxel. The cube contains multiple neighboring voxels with a particular size and shape. We move the cube through the entire measured brain volume, voxel by voxel. At each location, we measure the multivariate similarity between the time course from the voxels falling into the search cube and the time course from the voxels within the particular ROI. We can map the connectivity patterns of different spatial scales by choosing the search cube with different sizes and shapes (see Fig. 1).

To measure the similarity between two sets of multi-voxel time course, we use the multivariate statistic of RV coefficient. RV coefficient can be described as

$$RV(X, Y) = \frac{tr\left(XX^t YY^t\right)}{tr\left(XX^t XX^t\right)^{\frac{1}{2}} \times tr\left(YY^t YY^t\right)^{\frac{1}{2}}}. \qquad (1)$$

Two other equivalent formulas of RV-coefficient calculation are as follows:

$$RV(X, Y) = \frac{tr\left(YY^t XX^t\right)}{tr\left(X^t XX^t X\right)^{\frac{1}{2}} \times tr\left(Y^t YY^t Y\right)^{\frac{1}{2}}} \qquad (2)$$

$$RV(X, Y) = \frac{tr\left(Y^t XX^t Y\right)}{tr\left(XX^t XX^t\right)^{\frac{1}{2}} \times tr\left(YY^t YY^t\right)^{\frac{1}{2}}} \qquad (3)$$

where X and Y are $n \times p$ and $n \times q$ matrix from two data sets, which involve p and q numerical variables respectively on the same sample of n individuals, X^t is the transpose of matrix X, and $tr(\cdot)$ is the trace operator of square matrix.

When $p = q = 1$, the RV coefficient is the square of the Pearson correlation coefficient between the variables X and Y. When X is a single variable, and Y contains $q(q>1)$ variables, RV coefficient can be seen as an extension of the multiple correlation coefficient between X and the variables in Y. Many singular value decomposition (SVD)-based multivariate statistical methods, such as PCA (principal component analysis), CCA (canonical correlation analysis), MLM (multivariate linear regression analysis), PLS (Partial least square model analysis)
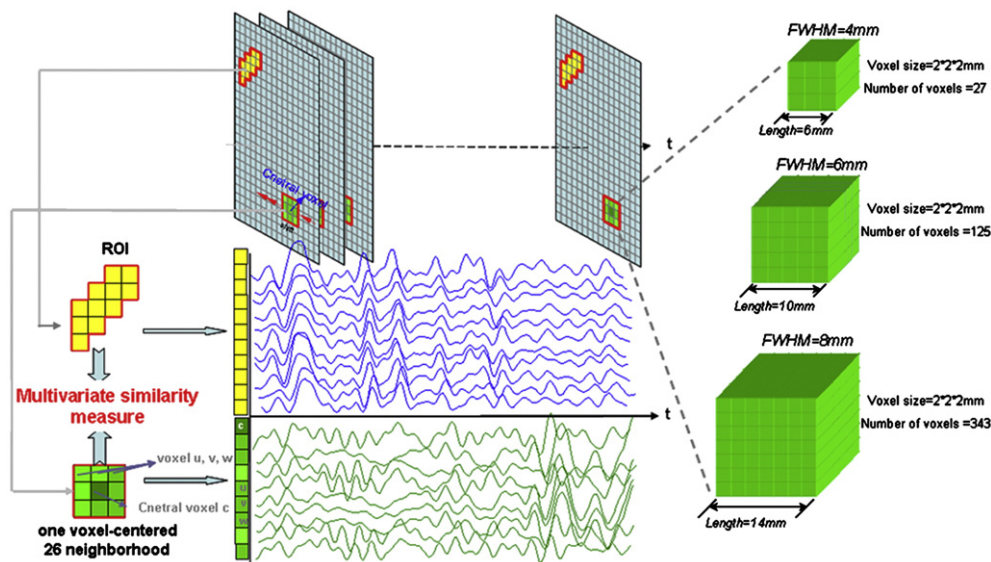
Fig. 1. The multivariate framework for the analysis of the functional connectivity. The yellow region surrounded by the red closed curve is the predefined region of interest (ROI). The blue region surrounded by the red closed curve is one of the local regions falling into the search cube. The search cube is moved through the entire brain volume voxel by voxel. At each location, the multivariate similarity is measured between the time course from the voxels within the search cube and the time course from the voxels within the ROI. (For interpretation of the references to color in this figure legend, the reader is referred to the web version of this article.)

and discriminant analysis can also be generalized within the framework of RV-coefficient problem (see also the Appendix B).

The value of RV coefficient ranges from 0 to 1. If RV coefficient is 0, the two sets are independent, which means there is no correlation or similarity between the two data sets. If RV coefficient is 1, the eigen components of data set X can be derived from Y through a homothetic transformation, which means that there exists a rotation matrix H and a scaling factor c such that $cXH = Y$. For RV calculation, X and Y must be mean centered by column first.

Multiple distance measure can also make use of the statistic of RV coefficient (Robert and Escoufier, 1976). For example, one kind of distance can be defined as:

$$D(X,Y) = \sqrt{2(1-RV(X,Y))} \tag{4}$$

where $D(X,Y)$ is the multiple distance between X and Y.

The RV coefficient's similarity measure and distance measure have already been successfully applied in analyzing fMRI data (Abdi et al., 2005, 2009; Abdi, 2007; Kherif et al., 2003; Shinkareva et al., 2006). Abdi et al. (2005, 2009) used RV coefficient to evaluate the similarity between distance matrix units in their multidimensional scaling method. Abdi (2007) also used RV coefficient to directly measure the similarity between two sets of multi-voxel time course. Kherif et al. (2003) adapted the RV coefficient with experimental paradigm and multidimensional scaling to investigate intersubject distances with respect to the comparison between activation and control. In Shinkareva et al.'s (2006) classification study, RV coefficient was used to generate dissimilarity maps for feature selection. While in the present study, we use RV coefficient to measure the spatial connectivity patterns between the region of interest and each local region of the whole brain.

The multivariate framework in this paper focuses on the analysis of fMRI data's local multi-voxels. Many local multivariate methods, based on their superior statistical properties than that of traditional univariate methods, have been used to analyze local region's spatial activation/connectivity pattern. In Friman et al. (2003)'s adaptive analysis method, CCA was used to automatically select each local region's optimal hemodynamic response and spatial filters under the prior constraint of a set of spatial basis functions and temporal functions. Harrison et al. (2003) use multivariate autoregressive (MAR) model to characterize the connectivity between a pair of local regions. Besides their different applications, the common purpose of these multivariate models is to use different constraint-condition (or called "prior knowledge") to obtain the suitable solutions for the model.

Weighted-RV for spatial fine-scale based temporal similarity measure

The RV coefficient is superior to the Pearson correlation coefficient in measuring the temporal similarities of two local brain regions: it combines information from local multi-voxels while maintaining the information about the fine-grain structure of the local region's spatial activation patterns. However, it is problematic to apply the RV coefficient directly to measure similarities between two brain regions: to maintain the fine-scale spatial information, the data cannot be smoothed; however, if smoothing is omitted, the spatial random noise in the data can significantly affect the detection performance of the fine-scale connectivity. There is another problem: within each localized search cube, the importance of all voxels is equal. This means that when we measure the similarity between the time course from ROI and the time course from a voxel-centered neighboring region, the importance of the central voxel will not be highlighted and weighted by the direct use of RV coefficient. This limitation can cause the boundaries of the functionally connected region to extend and the whole-brain connectivity maps become blurred. This point is illustrated in Fig. 1. In Fig. 1, the voxel c is located in the center of the search cube (the green region), the voxels u, v and w are involved in the cube but are located near the edge. If the center voxel c has very

weak synchronization of low-frequency oscillation with the ROI (the yellow region) in time course, while the voxels u, v and w have very strong synchronization of low-frequency oscillation with the ROI, the resulting connectivity map at voxel c is overestimated, and the similarity criterion is biased.

To address these two problems simultaneously, we borrow the idea of bilateral filtering (Tomasi and Manduchi, 1998; Rydell et al., 2006) in image processing. We gave different weights to the voxels within the search cube. We generate a weight template every time when the search cube moves to a new location. The size and shape of the weight template are the same as the search cube. We then add the template to the voxels within the search cube for the RV similarity measure. The generation of the weight template is based on two criteria: Euclidean distance to the central voxel and similarity of time course with that of the central voxel. According to these two criteria, we define two functions: the distance function $F_d(i,j)$ and the similarity function $F_s(i,j)$:

$$F_d(i,j) = F_d(d_{EU}(i,j)) \tag{5}$$

$$F_s(i,j) = F_s\left(d_{RV}\left(g_i,g_j\right)\right) \tag{6}$$

$d_{EU}(i,j)$ is the Euclidean distance between the voxel i and j. We specify (i_x,i_y,i_z) and (j_x,j_y,j_z) as the three-dimensional coordinate of voxel i and voxel j, then

$$d_{EU}(i,j) = \left((i_x-j_x)^2 + \left(i_y-j_y\right)^2 + (i_z-j_z)^2\right)^{\frac{1}{2}} \tag{7}$$

A simple and practical application of the distance function $F_d(i,j)$ is isotropic Gaussian function, which can be denoted as:

$$F_d(i,j) = \frac{1}{k_d}e^{-\frac{1}{2}\left(\frac{d_{EU}^2(i,j)}{\sigma_d^2}\right)} \tag{8}$$

k_d is the normalization constant of $F_d(i,j)$. σ_d is the standard deviation of the Gaussian kernel. The farther the distance of the voxel i and the voxel j, the smaller the value of the function $F_d(i,j)$. If we set voxel i as the central voxel in the region, this explicit expression of the closeness function $F_d(i,j)$ will give more weight to the central voxel and less weight to its neighboring voxels.

$d_{RV}(g_i,g_j)$ is RV dissimilarity measure which can be seen as another kind of distance between the observations of voxel i and j:

$$d_{RV}\left(g_i,g_j\right) = \sqrt{2\left(1-RV\left(g_i,g_j\right)\right)}$$

$$= \sqrt{2}\left(1-\frac{\left(n\sum_{t=1}^{n} g_{i,t}g_{j,t}-\sum_{t=1}^{n} g_{i,t}\sum_{t=1}^{n} g_{j,t}\right)^2}{\left(n\sum_{t=1}^{n} g_{i,t}^2-\left(\sum_{t=1}^{n} g_{i,t}\right)^2\right)\left(n\sum_{t=1}^{n} g_{j,t}^2-\left(\sum_{t=1}^{n} g_{j,t}\right)^2\right)}\right)^{\frac{1}{2}} \tag{9}$$

$g_{i,t}$ is the intensity of the voxel i at the observation of volume t.

Again, we use the Gaussian-type function, the similarity function $F_s(i,j)$ can be specified as:

$$F_s(i,j) = \frac{1}{k_s}r\left(g_i,g_j\right)e^{-\frac{1}{2}\left(\frac{d_{RV}^2\left(g_i,g_j\right)}{\sigma_s^2}\right)} \tag{10}$$

k_s the normalization constant of $F_s(i,j)$. σ_s is the standard deviation of the Gaussian kernel. $r(g_i,g_j)$ is the Pearson correlation coefficient. If the time course of voxel i and voxel j are highly similar, the value of the function is high, and the value approaches 1; on the contrary, if the time course of voxel i and voxel j are dissimilar and negatively

correlated, the value of the function approaches -1. Assuming voxel i is at the center of the search cube, this function will give more weight to the voxel j if it is more similar to voxel i at time course and less weight to voxel j if the two time course is dissimilar.

Then, functions (8) and (10) are combined into a new Gaussian-type function:

$$F_i(j) = F_d(i,j)^\alpha \cdot F_s(i,j)^\beta$$

$$= \frac{1}{k} r\left(g_i, g_j\right) e^{-\frac{1}{2}\left(\frac{\alpha\left(\left(i_x-j_x\right)2 + \left(i_y-j_y\right)^2 + \left(i_z-j_z\right)2\right)}{\sigma_d^2} + \frac{2\beta\left(1-RV\left(g_i,g_j\right)\right)}{\sigma_s^2}\right)}$$

$$(11)$$

In function (11), k is the normalization constant, which guarantee the discrete values of the Gaussian-type filter kernel add up to 1. The parameters α and β are used for balancing the effect of distance function and similarity function. The values of α and β range from 0 to 1, where 0 means no effect and 1 means full effect. If we want to put more emphasis on keeping homogeneous structure information within the searchlight and less emphasis on smoothing the data, we give larger value of α and smaller value of β, and vice versa.

In general, the weighted-RV calculation between the time course from ROI and the time course from central voxel i based each local region can be described as:

$$W_{-RV}(i) = RV(X, YF) \tag{12}$$

Here,

$$F = \begin{bmatrix} F_i(1) & 0 & \ldots & 0 \\ 0 & F_i(2) & & \ldots \\ \ldots & & \ldots & 0 \\ 0 & \ldots & 0 & F_i(q) \end{bmatrix}$$

X is $n \times p$ matrix from ROI, and Y is $n \times q$ matrix from central voxel i based neighborhood, F is $q \times q$ diagonal matrix which can be calculated using Formula (11).

The generation of the weight template is based on the numerical expression of the function (11) (see Fig. 2). Since the template combines the criterion of the spatial distance and the similarity of two voxels' time course, it can efficiently discriminate the spatial fine-scale feature information from the spatial random noise. Considering a $3 \times 3 \times 3$ search cube centered on voxel j, we use function (11) to generate a $3 \times 3 \times 3$ weight template. The voxels within the search cube are weighted differently according to the weight template. We use the RV coefficient to measure the similarity between the time course from the weighted voxels of the local region and the time course from the region of interest. To obtain a continuous functional-connectivity map, the cube is moved and centered on each voxel of the brain volume in turn. This method suppresses the spatial random noise and extracts the spatial connectivity information simultaneously. It can theoretically more efficiently detect the fine-grained structure of the functional-connectivity patterns. It should be noted that we select a cubic box window (search cube) sliding across the 3-dimensional volume. In fact, a cubic box window will produce absolutely identical results to a spherical window if the box window's side-length is identical to the spherical window's diameter. As for the search cube we use in our method, the voxels near the edge of the cube are always weighted zero in the weighted template, which means these voxels are never included as the filter passes across the whole volume.

Test for the significance of the RV coefficient

The distribution of the RV coefficient is unknown and thus we do not know a critical value to statistically test for similarity. The common strategy is to use no-parametric permutation test. However, due to the large number of observations in the fMRI data, exact permutation test is extremely time consuming (Mardia, 1971; Mielke, 1978, 1979; Hamani and Yves, 2007; Kubinger et al., 2007). Randomly sampling from the space of all possible permutations seems practical. In this case, however, the exact p-value depends on the number of random samples (Abdi, 2007; Josse et al., 2008).

In order to approximate the exact p-value as well as to reduce the computational intensity, a new statistic of normal distribution is approximated by log-transforming the first two moment of the RV coefficient's permutation distribution.

$$Z = \frac{\log\left(RV_{(X,Y)}\right) - E_{perm}\left(\log\left(RV_{(X,Y)}\right)\right)}{\sqrt{V_{perm}\left(\log\left(RV_{(X,Y)}\right)\right)}} \tag{13}$$

The log-transformation of the RV permutation distribution is suggested as a better normal approximation to obtain the real p-value without having to perform actual permutation (Heo and Gabriel, 1998; Josse et al., 2008) (see also the Appendix A). Thus, the computation cost is rather small. We adapt this z-distributed statistic to approximate the weighted-RV-coefficient map and test its significance. Finally, we adjust the significance levels using the FDR to solve the multiple comparison problems.

Simulated fMRI data

A simulation study was performed to compare the detecting performance of our weighted-RV method and the traditional ROI-based methods. To do so, the simulated resting-state fMRI data was generated in which the commonly used functional contrast-to-noise ratio (CNR), the temporal autocorrelation of the fMRI noise and the shape of the local regions with similar low-frequency fluctuations were known beforehand.

The description of the simulation

To generate the simulated data, we identify a priori the following: the foreground effect signals, five irregular shaped effect regions, and background noises. The foreground effect signal was extracted from actual EPI series which contain 200 observations (time points). The signal was then band-pass filtered within the range of 0.01–0.08Hz to simulate the low-frequency fluctuations of the BOLD signals in the resting state. We then varied the signal's phases between -4 to 4 TR to simulate different onsets of the hemodynamic responses. The time course of the background noise was generated by making use of the fractional Gaussian noise (fGn) model (Maxim et al., 2005), and the Hurst exponent was used to characterize the temporal autocorrelation of the fMRI time signal. The background noise was a time course of a 3-dimensional volume, which had the same number of observations as that of the foreground effect signals. For each volume, TR = 2s, slice = 20, voxel sizes = $2 \times 2 \times 2$ mm, matrix = 64×64.

Five irregular shaped effect regions were created by making use of the region growing method. These local regions comprised of 10, 30, 90, 180 and 270 voxels respectively. These five irregular shaped local regions were embedded in different places of the background volume. Within these local regions, the foreground effect signals with varied TR value were added to the background noise at different functional contrast-to-noise ratio (CNR). The functional contrast-to-noise ratio (CNR) was defined as the spatial average within the effect region of the absolute activity level at the maximum of the hemodynamic response divided by the temporal standard deviation of the noise. The foreground signals were associated with fine-scale patterns of weak connectivity effect presented in the real fMRI data. Outside these regions, there were no foreground effect signals and only background noises (Fig. 3).
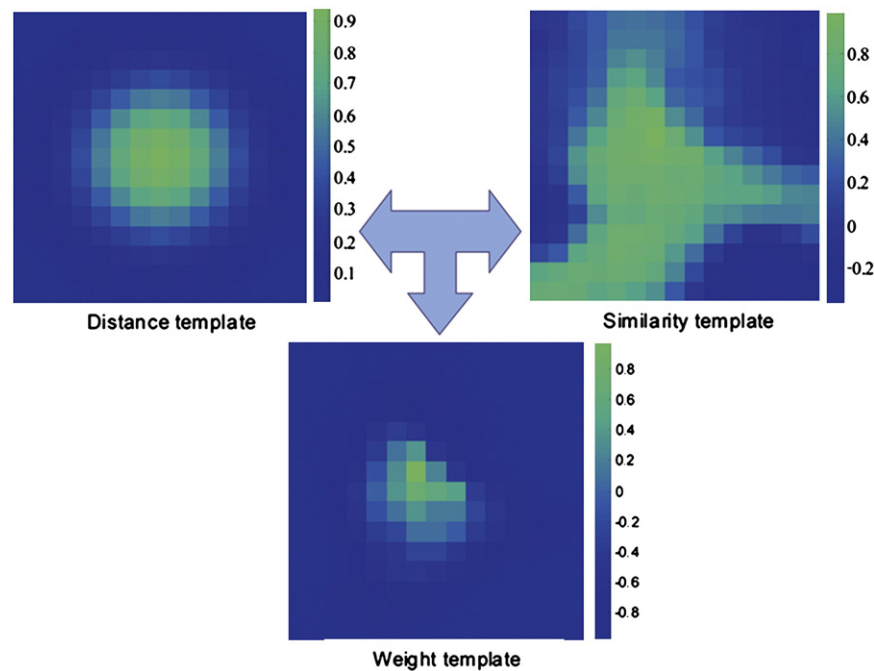
Fig. 2. The weight template is constructed by multiplying the distance template with the similarity template. The distance template is generated from isotropic Gaussian function (see Formula 8), which has more weight in the central voxels and less weight at the edge. The similarity template is generated from a Gaussian-type similarity function (see Formula 10), which has more weight to voxels if they are more similar to the central voxels at time course and less weight to voxels if they are dissimilar to the central voxels at time course.

Analysis of the simulated data

The following four types of analytic methods were used to map the whole-brain functional connectivity:

(1) Pearson correlation analysis on unsmoothed fMRI data
(2) Pearson correlation analysis on smoothed fMRI data
(3) Direct RV analysis on unsmoothed fMRI data
(4) Weighted-RV analysis on unsmoothed fMRI data

In Methods (2) ("Methods (2)" here represent a class of methods with varied Gaussian kernel), the full width at half maximum (FWHM) of the Gaussian kernel for smoothing were 4 mm, 6 mm and 8 mm respectively.

The variances of all Gaussian kernels were 1. In Methods (3) ("Methods (3)" represent a class of methods with varied search cube) and Methods (4), the size of the search cubes were 6 mm×6 mm×6 mm ($3\times3\times3$ voxels), 10 mm×10 mm×10 mm ($5\times5\times5$ voxels) and 14 mm×14 mm×14 mm ($7\times7\times7$ voxels). The values of σ_d, σ_s, α and β were set to 1. These parameter sets guaranteed the Gaussian kernel for smoothing in Methods (2) to be corresponding to the search cubes in Methods (3) and (4). For the simulated data, we set the constant value of the Hurst exponent to be 0.8 as generating the background noise, and this guarantee the time course of fMRI were positively autocorrelated (Maxim et al., 2005). The functional contrast-to-noise ratio (CNR) was varied at six different values (CNR = 0.1, 0.2, 0.3, 0.4, 0.5, 0.6). Fig. 4
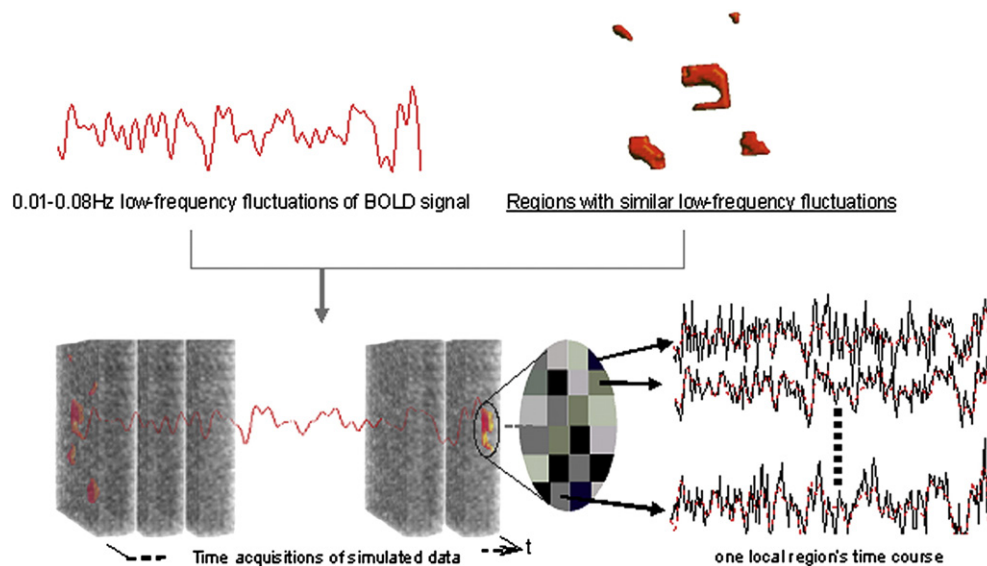
Fig. 3. The simulation of fMRI data during the resting state. In this simulated data, five irregularly shaped local regions with similar low-frequency fluctuations are predefined and embedded in the 3-dimensional background noise. Within the local regions, the time course is the mixture of foreground effect signal and background noise at different functional contrast-to-noise ratios (CNR). Outside these regions, there is no foreground effect signal but only background noise.
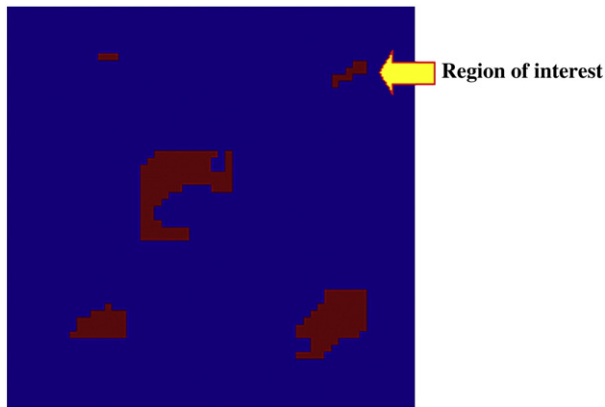
Fig. 4. The effect regions of the 3-dimensional simulated data in the middle slice. The red regions show that these regions have similar low-frequency fluctuations at time course. The blue region shows that there is only background noise content and has no effect. (For interpretation of the references to color in this figure legend, the reader is referred to the web version of this article.)

shows the five irregular local regions with low-frequency functional connectivity in the simulated data. The local region 2 containing 30 voxels was selected as the region of interest during the analysis.

Results of simulation

Fig. 5 shows the unthresholded mapping results obtained with different methods for the simulated fMRI data (CNR = 0.4). It can be seen that the Pearson correlation analysis without any smoothing of the data (i.e., Method 1) could detect some voxels which have connectivity with the region of interest, while the connectivity maps show a severe salt-and-pepper phenomenon (Fig. 5A). This is inconsistent with the hypothesis that the functional region of the brain is clustered and locally homogeneous (Zang et al., 2004).

The Pearson correlation analysis on the smoothed fMRI data (i.e., Methods (2)) resulted in focal regions in the connectivity map. However, the fine-scale connectivity information within the map was somewhat lost, and the boundaries of the connected regions related to the regions of interest were blurred and ambiguous (Fig. 5B). This suggests that although smoothing the data with Gaussian kernel could suppress the spatial noise and improve the homogeneity of nearby voxels, it had the difficulty in distinguishing the signals from the random noises, rendering the former as the noise and being eliminated from the final connectivity map. Direct RV calculation on unsmoothed fMRI data also got clustered effect regions in the connectivity maps (Fig. 5C), however, similar to the results of Methods (2), the boundaries of the effect regions in the maps were blurred, and the fine-scale information of the maps were seriously contaminated. Furthermore, from the maps we can see that the contrast between the detected effect regions and background noise were very low, which indicate the low signal to noise ratio of Methods (3). In contrast, the functional-connectivity map shown in Fig. 5D illustrates that the weighted-RV analysis produced relatively the optimal performance at detecting the fine-scale based local regions which have highly similar low-frequency fluctuations with the region of interest.

To quantitatively assess how well different methods distinguish between the effect regions (the five irregular local regions which have similar low-frequency fluctuations) and the background noise, we use receiver-operating characteristics (ROCs; Fig. 6). The ROC curve is defined as the proportion of correctly detected voxels among all effect-region voxels (the sensitivity) and the proportion of correctly rejected voxels among all pure-noise voxels (the specificity) at all possible thresholds. As shown in Fig. 6, the curves of Methods (2) are at the bottom of all curves, which indicates the worst performance. This is because smoothing the original fMRI data filters out the fine-scale information component of the data and reduces the detection performance. The ROC curves also show that the effect of different sizes of the Gaussian kernel has on detection performance. The wider the kernel window, the worse is the detection performance. This is due to the fact that different Gaussian windows represent the different levels of low-pass filters with the wider Gaussian kernels filtering out more information. The curves of Methods (3) are located above that of Methods (2), and this indicate the direct RV calculation on unsmoothed data performs better than the traditional Pearson correlation analysis on smoothed data. Combining the ROC-curve illustrations with the unthresholded maps of Fig. 5C, we see that the multivariate RV measure can keep the local structure of the connectivity patterns and suppress the spatial random noise to a certain extent, while it does not perform well on detecting those very subtle connectivity information seriously contaminated by the noise. The curves of Methods (4) are located on the top of all curves which indicate the best performance. By combining multiple signals of neighboring voxels within the search cube, the weighted-RV method can make full use of the spatial structure information while at the same time it can effectively suppress the spatial noise.

A few additional points are worth noting. At very low functional contrast-to-noise ratio (CNR), which means the fMRI data is seriously contaminated with noise, Methods (4) can still detect some weak effects of the connectivity patterns, whereas Methods 1, 2 and 3 perform poorly. For Methods (2), the Pearson correlation analysis on smoothed data with FWHM = 4 mm achieves the relatively better performance compared to the other two methods with 6 mm and 8 mm FWHM. This shows once again that wider Gaussian kernels filter out more fine-grained feature information of the data. Of all size of the search cubes and analysis methods, the weighted-RV analysis method with 6 mm × 6 mm × 6 mm search cube is the most sensitive and achieves the best performance in detecting the irregular functional-connected local regions. This is perhaps due to the fact that the region of interest we chose comprised of 30 voxels, and this voxel number is closest to the voxel number of the search cube containing 27 voxels.

Connectivity of the motor cortex in resting state: real fMRI data verification

We used real resting-state fMRI data to obtain functional-connectivity maps with the use of the three methods described above.

Subjects and measurements

Eight healthy subjects (3 male, 5 female, and age from 50 to 67) participated with informed consent. The study was approved by the research ethics committee at the Tiantan Hospital.

The experiment consisted of 2 phases. In the first phase, a resting scan was obtained. Participants who were unaware of the exact experimental design were instructed to lie with their eyes closed, think of nothing in particular, and not fall asleep. In the second phase, a right finger movement task was performed. During this phase, the right

Fig. 5. Unthresholded mapping results obtained with different methods for the simulated fMRI data (CNR = 0.4, Hurst exponent = 0.8). A. The map obtained with Pearson correlation analysis on unsmoothed fMRI data. B. The maps obtained with Pearson correlation analysis on smoothed fMRI data with FWHM = 4 mm (left); 6 mm (middle); and 8 mm (right). $\sigma = 1$. C. The maps obtained with direct RV analysis on unsmoothed fMRI data with 6 mm × 6 mm × 6 mm search cube (left); 10 mm × 10 mm × 10 mm search cube (middle); and 14 mm × 14 mm × 14 mm search cube (right). $\sigma_d = 1, \sigma_s = 1, \alpha = 1$, and $\beta = 1$. D. The maps obtained with weighted-RV analysis on unsmoothed fMRI data with 6 mm × 6 mm × 6 mm search cube (left); 10 mm × 10 mm × 10 mm search cube (middle); and 14 mm × 14 mm × 14 mm search cube (right). $\sigma_d = 1, \sigma_s = 1, \alpha = 1$, and $\beta = 1$.
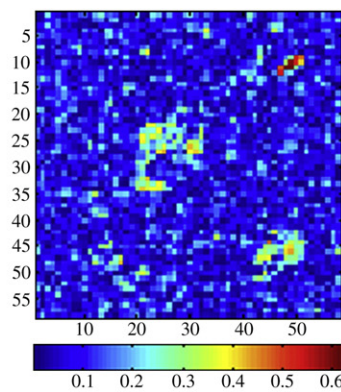
A The map obtained with Method(1)
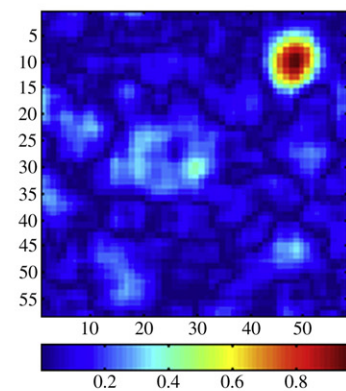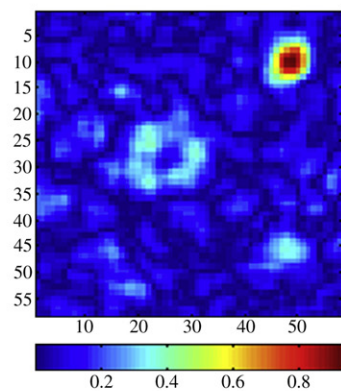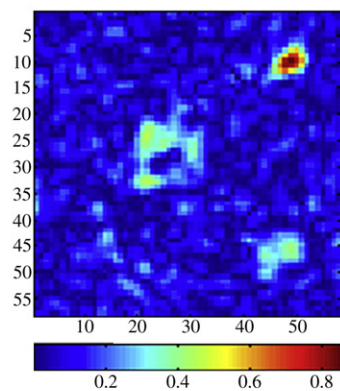
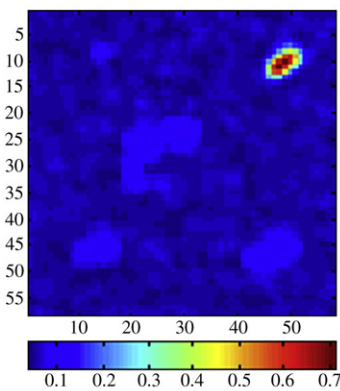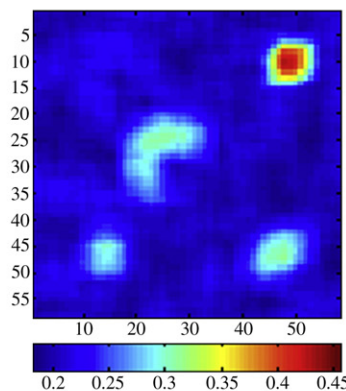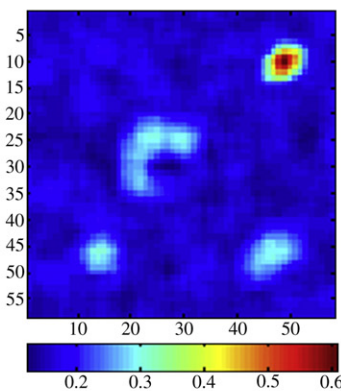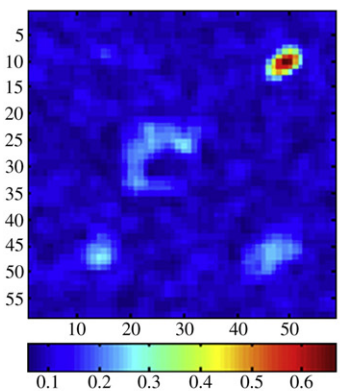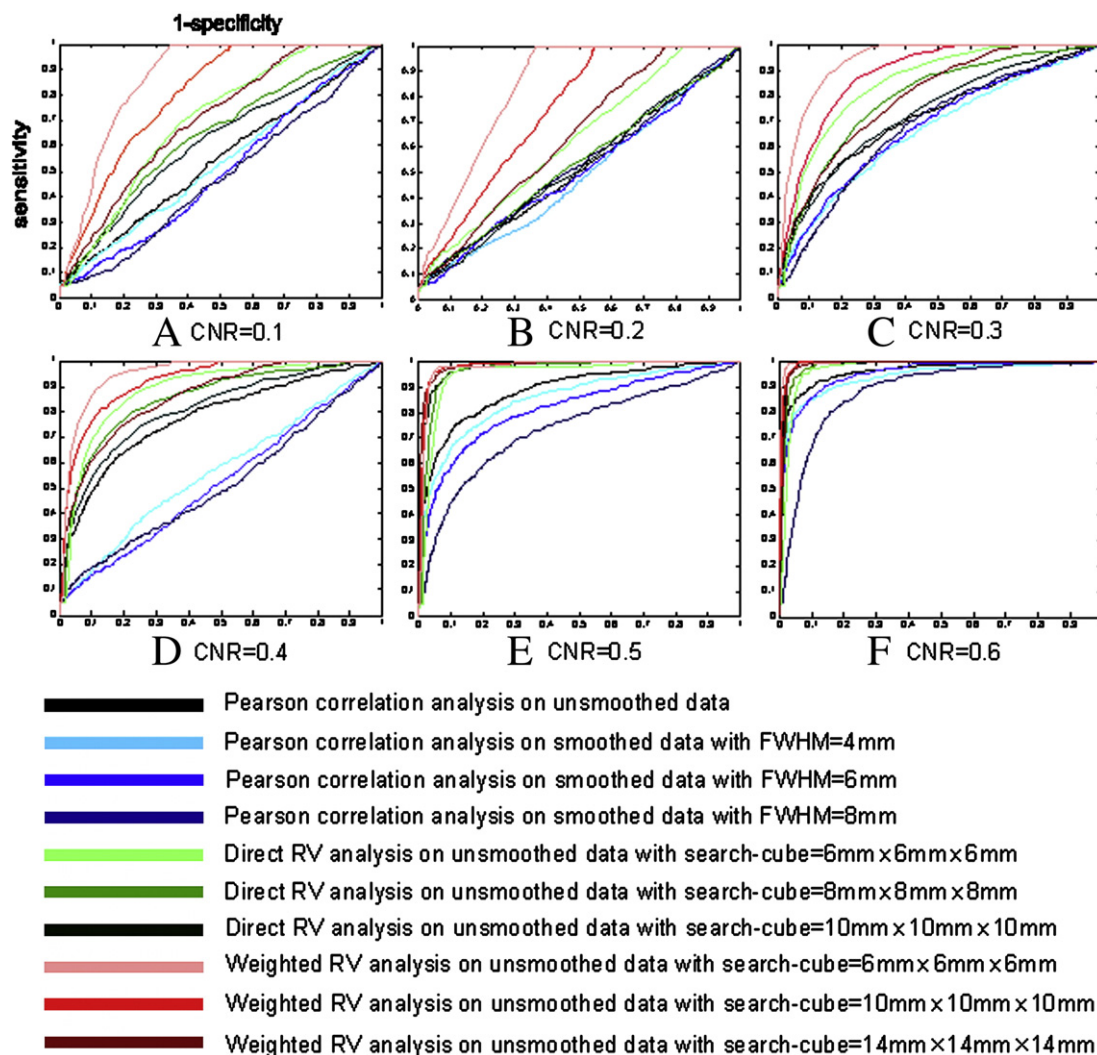B The map obtained with Methods(2)
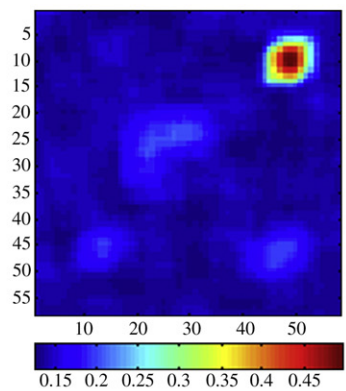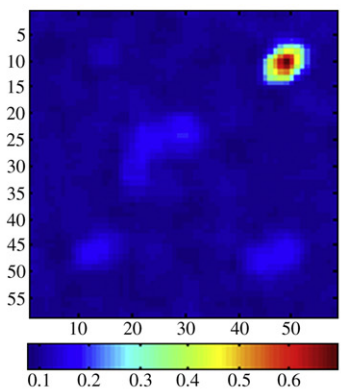
C The map obtained with Methods(3)

D The map obtained with Methods(4)

Fig. 6. The ROC curves for different methods: the curves for Pearson correlation analysis on unsmoothed fMRI data (black); the curves for Pearson correlation analysis on smoothed fMRI data with FWHM = 4 mm (light blue), FWHM = 6 mm (blue) and FWHM = 8 mm (dark blue); the curves for direct RV analysis on unsmoothed fMRI data with 6 mm × 6 mm × 6 mm search cube (light green); 10 mm × 10 mm × 10 mm search cube (green); 14 mm × 14 mm × 14 mm search cube (dark green). the curves for the weighted-RV on unsmoothed fMRI data with 6 mm × 6 mm × 6 mm search cube (pink), 10 mm × 10 mm × 10 mm search cube (red) and 14 mm × 14 mm × 14 mm search cube (brown); the simulation use constant value of Hurst exponent (H = 0.8) and six different functional contrast-to-noise ratios: (A) CNR = 0.1, (B) CNR = 0.2, (C) CNR = 0.3, (D) CNR = 0.4, (E) CNR = 0.5, and (F) CNR = 0.6. (For interpretation of the references to color in this figure legend, the reader is referred to the web version of this article.)

sequential finger movement epochs and rest epochs were performed alternatively, each replicated 4 times. The task was implemented in a standard block design. The fMRI scan of the task in Phase 2 was used to accurately localize each individual's motor region of interest (ROI) within the left primary motor cortex (or called "M1"). The selection of local region within the left primary motor cortex as region of interest (ROI) is due to the reason that this functional area of the brain is always reported to be involved in motor tasks (Terumitsu et al., 2009; Damoiseaux et al., 2006; Jiang et al., 2004; Biswal et al., 1995; Lowe et al., 1998; Xiong et al., 1999). Each individual's region of interest (ROI) was then used for analyzing the spatial fine-scale based functional connectivity during the resting state. Each scan session lasted 4 minutes.

Structural and functional MRI were collected using a 3.0 T MR imaging system (Siemens Trio Tim). The fMRI series were collected using a single shot, T2*-weighted gradient-echo echo planar imaging (EPI) sequence (TR = 3000 ms; 36 slices, 4 mm thickness; matrix = 64 × 64) covering the whole brain with a resolution of 3.75 × 3.75 mm. High-resolution anatomical scans were acquired with a three-dimensional enhanced fast gradient-echo sequence (TR/TE = 8.516/3.4 ms, matrix = 256 × 256), recording 156 axial images with a thickness of 1 mm and a resolution of 1 × 1 mm.

Preprocessing was performed on each subject's two fMRI sessions: The first three volumes of each fMRI scan were discarded. Scans were slice timing corrected, spatially realigned, normalized into the standard MNI atlas space according to the segmented grey images, re-sampled to 2 mm cube voxels, global proportionally scaled to yield a whole-brain intensity value of 1000. For the scan of the task in Phase 2, it was high-pass filtered to correct the low-frequency drift in the BOLD signals. The volumes of the scan were spatially smoothed with a full width of 4 mm at half maximum. The scan was then entered into the General Linear Models (GLM) for parameter estimation. By comparing the finger-movement condition with the rest condition, a small active region was localized in the right primary motor cortex (p < 0.001, FDR corrected, number of contingent voxels > 15). Since this functional region included only the voxels that were significantly activated during the right finger movement task, this irregular region was defined as the ROI for analysis of connectivity in resting state (see Fig. 7). For the resting scan, it was 0.01–0.08Hz band-pass filtered by using the discrete-cosine-transform (DCT) to retain the low-frequency fluctuations (LFF) signal only. All the procedure was implemented with SPM5 software (www.fil.ion.ucl.ac.uk/spm/) and in-house Matlab codes.

Data analysis and method comparisons

To compare the performance of the weighted-RV and the traditional ROI-based methods in detecting the fine-scale structure of the functional-connectivity patterns, we analyzed the functional-connectivity map of the motor related brain network during the resting state by using the following three methods:

(1) Pearson correlation analysis on unsmoothed resting scan;
(2) Pearson correlation analysis on smoothed resting scan with FWHM = 6 mm;
(3) Weighted-RV analysis on unsmoothed resting scan with search cube = 5 mm × 5 mm × 5 mm.

In Method 2, the variance of Gaussian kernel was 1. In Method 3, the values of parameters σ_d, σ_s, α and β were set to be 1. Here we selected the Gaussian kernel of 6 mm FWHM in Method 2 and the search cube of 5 mm × 5 mm × 5 mm size in Method 3 for comparison. This was because that the two methods have same statistical power in combing the signals of their neighbor voxels, and that our region of interest contained the closest number of voxels (number of voxels = 118) with the Gaussian kernel and search cube (number of voxels = 125). To find the distributed functional regions that have significant connectivity with the motor region of interest, significant tests must be performed on the statistical parametric maps (Pearson correlation coefficient map obtained with Method 1 and 2 and the weighted-RV-coefficient map obtained with Method 3). Here, the weighted-RV map was transformed to the normal distributed map by using Formula (13) (see Test for the significance of the RV coefficient). For explicit comparison, the Pearson correlation map was also transformed to the z-score map by using Fisher's z transformation (Fox et al., 2005). Finally, for the above three connectivity maps, the significance levels were adjusted by using the false-discovery-rate (FDR) to solve the multiple comparisons problem (p<0.01, FDR corrected, number of contingent voxel>1).

Results of real fMRI data

Fig. 8 shows the connectivity map obtained with the above three methods. Three connectivity maps all show that, during the resting state, the left primary motor areas have significant low-frequency connectivity with the following regions: the right primary motor area (M1), the supplementary motor area (SMA), the bilateral primary sensory cortex (S1), and the areas in the bilateral posterior parietal
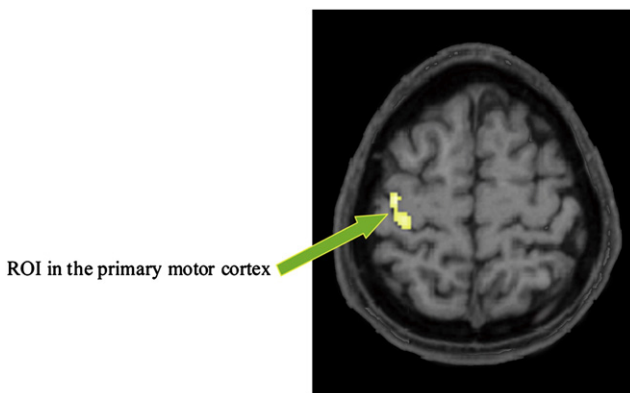
Fig. 7. The localized region of interest (green arrow) in the left primary motor cortex for a single subject by comparing the right finger movement condition with the rest condition (p<0.001, FDR corrected, number of voxels>15). (For interpretation of the references to color in this figure legend, the reader is referred to the web version of this article.)

cortex and left anterior cerebellum. However, the connectivity map obtained with Method 1 shows a salt-and-pepper pattern, which makes it difficult to distinguish the actual connectivity patterns from the spatial noise. The connectivity map obtained with Method 2 is homogeneous within a particular local region. This suggests that Method 2 removed some spatial random noise and make the connected regions more localized. However, a large number of the fine-scale patterns of low-frequency connectivity may have been lost. In contrast, like our simulation results, Method 3 appeared to obtain relatively the optimal performance in detecting the spatial fine structure of the connectivity patterns.

The performance of the above three methods can also be illustrated by focusing on three small local areas from the three different connectivity maps. From the local area (A) in Fig. 8, there are no significantly connected voxels in Maps 2 and 3 but exist in Map 1 likely due to spatial noise. Since Methods 2 and 3 contain the steps of spatial denoising, these noise voxels are well suppressed. From the local area (B) in Fig. 8, significantly connected local regions obtained with Method 2 are larger than those obtained with Methods 1 and 3. This is likely due to the fact that Method 2 combined the local multiple voxels without distinguishing the noise and feature information, and thus the functional-connected regions are extended and the border of the regions is blurred. From the local area (C) in Fig. 8, we can clearly see that Method 3 precisely extracted the fine-scaled based spatial connectivity patterns while Methods 1 and 2 failed to do so.

Group mean of the 8 subjects' connectivity maps revealed that, of all voxels marked significant, 64.1% (SD = 17.2%) were marked significant in the map obtained with Method 1, 66.5% (SD = 19.6%) were marked significant in the map obtained with Method 2, and 68.1% (SD = 23.2%) were marked significant in the map obtained with Method 3. Only 37.1% (SD = 15.5%) were marked significant in maps obtained with the above three methods (see Fig. 9). This means that the above three methods shared some common properties in detecting resting-state motor network. However, at fine scales, detecting performance of these methods varied substantially.

Of all voxels marked significant in either map, 9% (SD = 4%) were marked in map obtained with Method 1 but not in maps obtained with Methods 2 and 3. This kind of voxels was most likely to be false positive voxels caused by spatial random noise because smoothing and feature-preserved filtering both exclude these voxels well. Of all voxels marked in either map, 12.5% (SD = 6.7%) were marked significant only in the map obtained with Method 2 but not in the map obtained with Methods 1 and 3. This kind of voxels was also highly suspected to be false positive voxels because smoothing of the data often extends some functionally correlated regions. Of all voxels marked significant, 16.3% (SD = 6.4%) were marked significant only in the map obtained with Method 3. These voxels most probably reflected the fine-scale patterns of connectivity information, which were not detected by using Methods 1 and 2. 9.8% (SD = 3.2%) of all marked voxels exist in the maps obtained with Methods 1 and 2 but not in the map obtained with Method 3. We are more inclined to think these were true positive voxels not only because these voxels passed through non-smoothing (Method 1) and smoothing (Method 2) correlation analyses, but also because our weighted-RV methods (Method 3) were not accurate enough at present to detect all the positive voxels. Finally, results of one-sample t-test group analysis of each method's Z-maps were shown in Fig. 10 (p<0.05, FDR corrected).

Discussion

To date, the investigation of resting-state functional connectivity can be roughly classified into two categories: the ROI-based correlation analysis and the singular value decomposition (SVD)-based component analysis (also known as "data-driven" methods). The "data-driven" methods, such as principal component analysis (PCA), independent
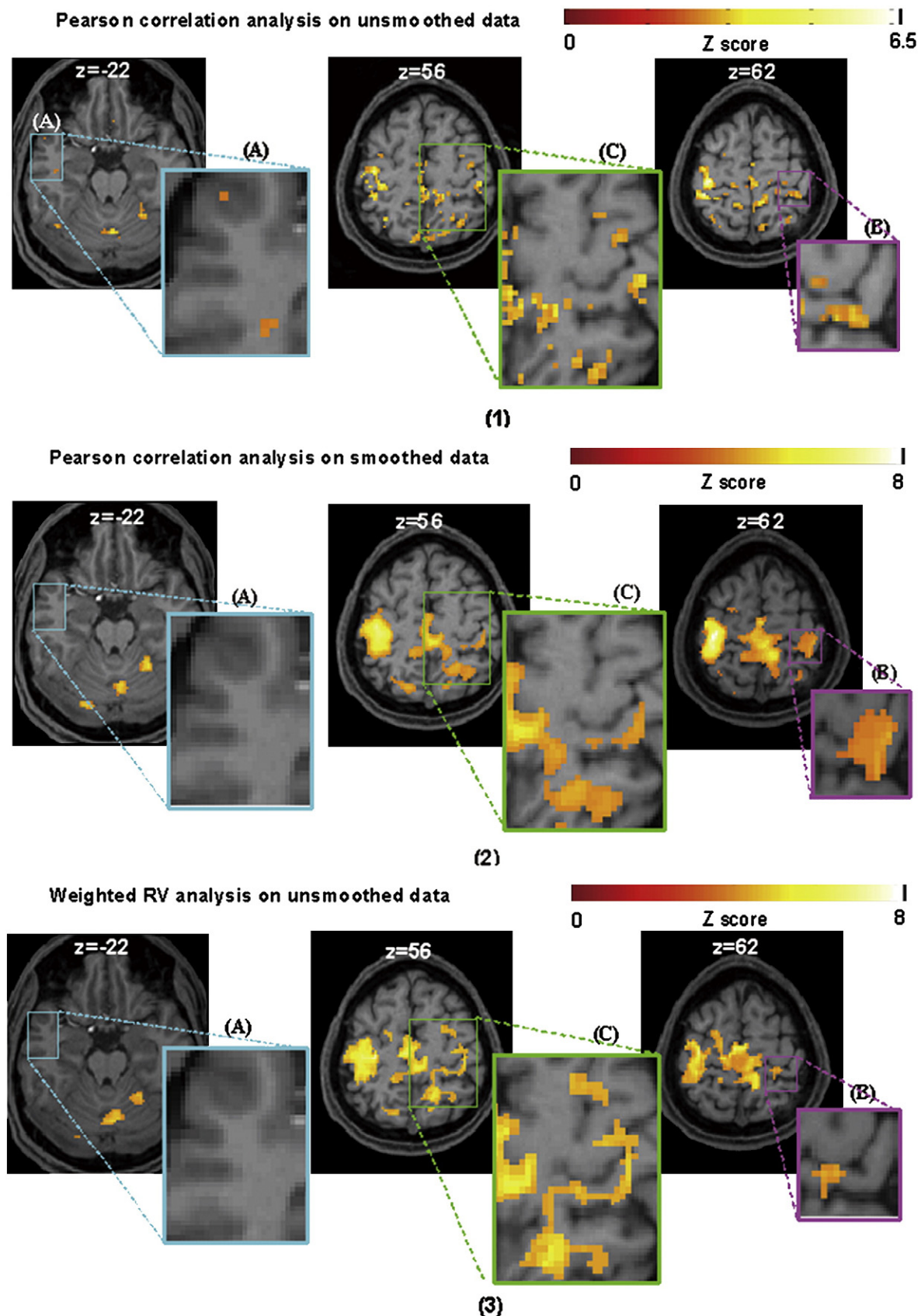
Fig. 8. The functional-connectivity map of the motor network during the resting state. $p<0.01$, FDR corrected, number of contingent voxel>1. (1) Maps obtained with Pearson correlation analysis on unsmoothed resting scan; (2) maps obtained with Pearson correlation analysis on smoothed resting scan with FWHM = 6 mm; (3) maps obtained with weighted-RV analysis on unsmoothed resting scan with search cube = 5 mm × 5 mm × 5 mm.
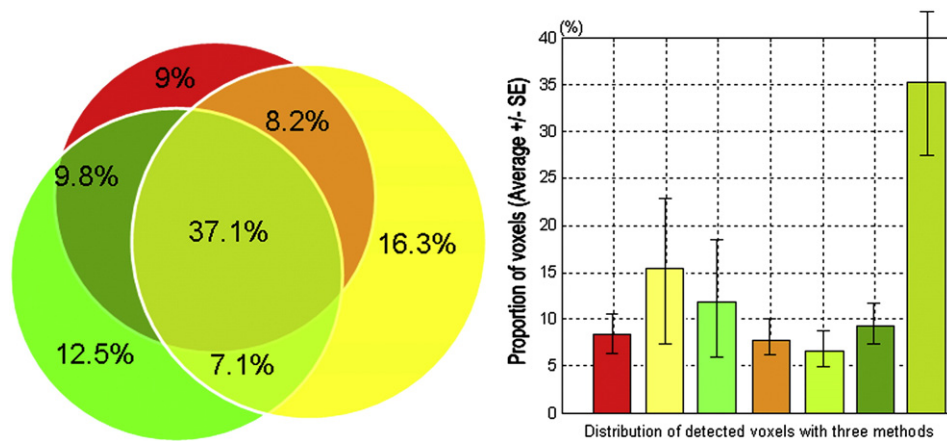
Fig. 9. Group mean of 8 subjects' connectivity maps. The average proportions of the voxels detected with Method 1 (red); the average proportions of the voxels detected with Method 2 (green); the average proportions of the voxels detected with Method 3 (yellow); the average proportions of the voxels detected with Methods 1 and 2 (dark green); the average proportions of the voxels detected with Methods 1 and 3 (orange); the average proportions of the voxels detected with Methods 2 and 3 (green yellow); the average proportions of the voxels detected with Methods 2 and 3 (olive green). Of all voxels marked significant in either connectivity map, 9% (SD = 4%) are marked significant only in the map obtained with Method 1; 12.5% (SD = 6.7%) are marked significant only in the map obtained with Method 2; 16.3% (SD = 6.4%) are marked significant only in the map obtained with Method 3; 9.8% (SD = 3.2%) are marked significant in maps obtained with Methods 1 and 2; 8.2% (SD = 2.7%) are marked significant in maps obtained with Methods 1 and 3; 7.1% (SD = 2.6%) are marked significant in maps obtained with Methods 2 and 3; 37.1% (SD = 15.5%) are marked significant in maps obtained with the three methods. (For interpretation of the references to color in this figure legend, the reader is referred to the web version of this article.)

component analysis (ICA: Damoiseaux et al., 2006; Beckmann et al., 2005), canonical correlation analysis (CCA: Nandy and Cordes, 2004; Ragnehed et al., 2009) and partial least squares (PLS: McIntosh et al., 2004), have achieved great success in simultaneously extracting a variety of functional-connectivity maps. However, despite their many advantages, the major limitation of these methods is their difficulty in explaining the function of every decomposed connectivity map. Also, it is hard to distinguish the results due to the spatial random noises and those due to some fine-grained patterns of connectivity maps. In contrast, the ROI-based correlation analysis is used for directly detecting a function-specialized network (Biswal et al., 1995; Lowe et al., 1998; Greicius et al., 2003; Fox et al., 2005; Bokde et al., 2006). By predefining a functionally specialized ROI and measuring the correlation between the BOLD time course from the ROI and the time course from all other local regions in the brain, we can explicitly obtain the connectivity between these functionally related brain regions within a functionally specialized brain network we are focusing on. For the above reasons, we prefer ROI-based methods for obtaining functionally specialized brain networks in the resting state.[1]

In this paper, we develop an ROI-based multivariate statistical framework for the analysis of the low-frequency functional connectivity of brain network during the resting state. Under this framework, the weighted-RV method is proposed to detect the spatial fine-scale patterns of functional connectivity. Simulation and real fMRI experiment both show that the weighted-RV method achieves much better performance in mapping the fine-grained patterns of functionally specialized brain network compared to the traditional ROI-based methods. The success of this method is due to two reasons: one is that we use local multivariate voxels instead of one single voxel for measuring its synchronization of low-frequency BOLD fluctuations with ROI, so more information of local spatial structure is kept. The other is that we use a strategy similar to bilateral filter to give different voxels within the search cube different weights when performing multivariate similarity measure. This strategy can well suppress the spatial random noise as well as extract the fine-grained structure of the connectivity patterns, so it is

more sensitive in detecting the fine-scale low-frequency connectivity even at a very low functional contrast-to-noise ratio (CNR).

The exploration of the fine-scale functional connectivity relies on advancement of two aspects: high-resolution functional magnetic resonance imaging (fMRI) technique and the advanced data analysis method. The 3.0 T or higher field magnetic resonance imaging technique provides us with a large amount of data containing fine-scale based spatial information. By using the advanced data analysis method such as the weighted-RV proposed here, we can make full use of the spatial information to capture the fine-grained spatial structure of functional connectivity.

In the real fMRI experiment, we extracted the functional connectivity of the motor cortex during the resting state, an issue that has been studied extensively. Our result is consistent with the findings of these previous studies using the traditional ROI-based univariate analysis method (Biswal et al., 1995; Xiong et al., 1999), as well as the findings using the ICA methods (Damoiseaux et al., 2006; Robinson et al., 2009). However, at the fine scale, our result appeared to provide more spatial fine-scale patterns of functional connectivity that were not clearly observed previously.

The weighted-RV method can be further improved. In this paper, the RV coefficient map is tested by using the parametric permutation test. The advantage of this kind of test is the low computational cost while at the same time providing a reasonable estimation of the p-values. However, there are also some novel tests that are more sensitive in testing cluster based statistics. For example, Poline et al. (1997) developed a voxel-and -cluster-combined test based on the Gaussian random field theory. Bullmore et al. (1999) used maximum cluster mass as a statistic to perform the permutation test. Hayasaka and Nichols' (2004) combined voxel–cluster size tests are also sensitive and perform well in testing cluster based statistics. These tests can also be utilized in the future to test the significance of the RV coefficient map to improve statistical sensitivity.

RV coefficient is clearly a suitable multivariate statistic to measure the similarity between two sets of BOLD signals. However, it should not be construed as the only multivariate statistic that is capable of achieving the performance obtained in the present study. Under the multivariate statistical framework constructed in this paper, other multivariate statistic for similarity can also be utilized, such as the canonical correlation coefficient. In this paper, our weighted-RV method can well suppress the spatial random noise and enhance the detectability of the fine-scale spatial functional-connectivity

---

[1] Other methods focus on evaluating the interregional connectivity of all predefined ROIs (Harrison et al., 2003; Gitelman et al., 2003; Cordes et al., 2002; Salvador et al., 2005; Achard et al., 2006). This kind of methods is not usually used for *detecting* whole brain network, so we do not discuss it further here.
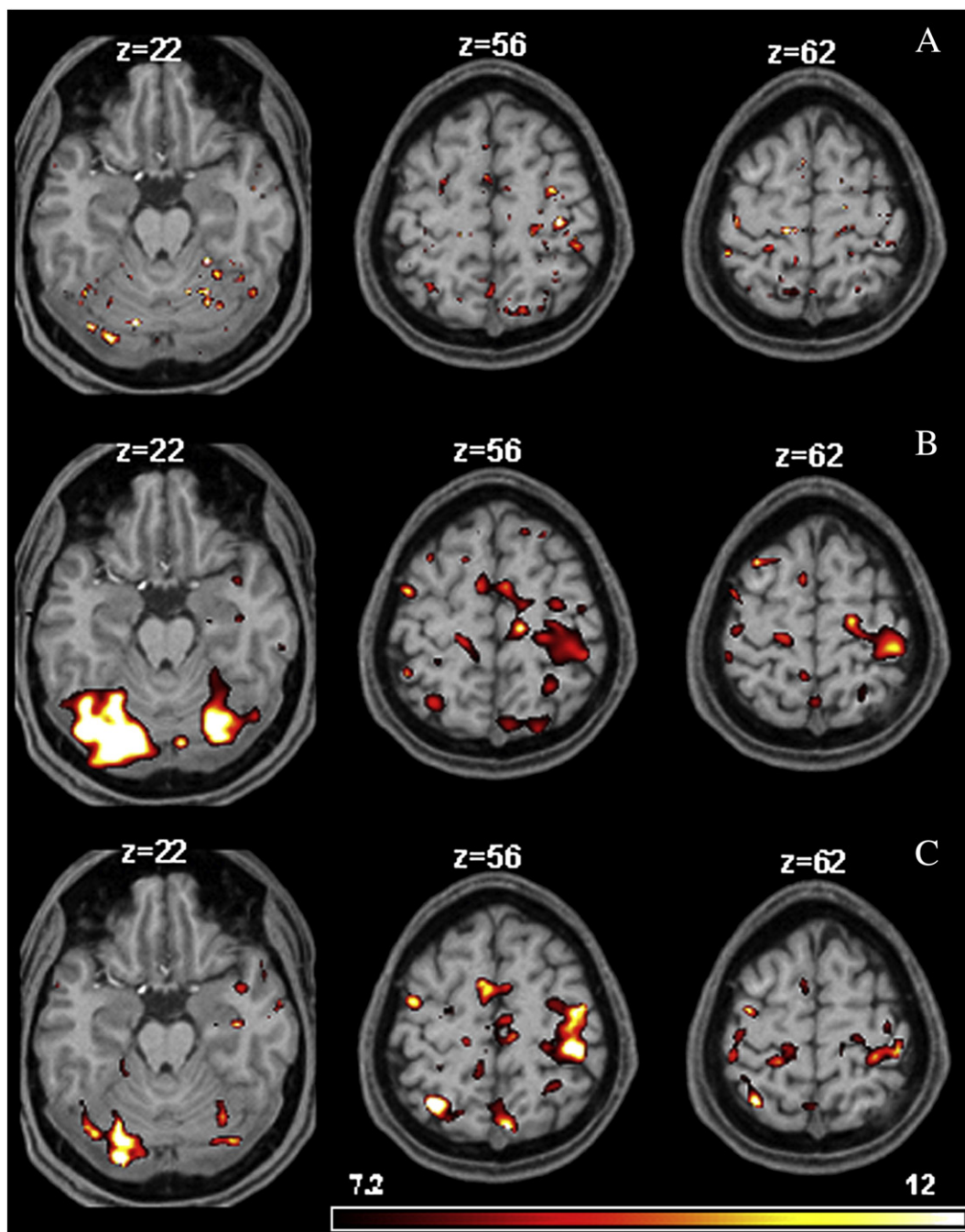
Fig. 10. The one-sample t-test analysis of (A) Pearson correlation analysis on unsmoothed data; (B) Pearson correlation analysis on smoothed data; (C) weighted-RV analysis on unsmoothed data. $p < 0.05$, FDR corrected, number of contingent voxel > 1.

information, which is achieved by the integration of the bilateral filtering to the multivariate statistical framework. In view of this, more advanced feature-preserving denoising methods can also be considered and integrated into our multivariate framework. The application of the weighted-RV focuses on detecting the resting-state functional connectivity in this paper. However, it can also be extended to detect special task induced fine-scale functional connectivity, which needs to be explored in the near future.

Appendix A

The test used in this article is to approximate the permutation distribution by a continuous distribution under the null hypothesis that the data sets X and Y (see The multivariate framework for the analysis of functional connectivity) are independent. In 1995, Kazi-Aoual et al. (1995) gave the explicit expressions for the first two moments of the permuted RV coefficient. Considering the RV permutation distribution is markedly skewed to the right, Heo and Gabriel (1998) used the log-

transformation of the RV's first two moment to obtain an approximately normal distribution.

Let: $X = (x_1, x_2, ..., x_n)^t$, $Y = (y_1, y_2, ..., y_n)^t$, $A = XX^T$, $B = YY^T$. $X_{(n \times p)}$ and $Y_{(n \times q)}$ must be mean-centered by column. If it is not mean centered, it can be transformed in the following way:

$$\left(I_n - \left(\frac{1}{n} \right) 1_n 1_n^T \right) X = X - \left(\frac{1}{n} \right) 1_n 1_n^T X \quad (A.1)$$

where I_n is the identity matrix of size n and 1_n is the column-vector of n ones.

The mathematical expectation of permutated $RV(X, Y)$ is calculated as follows:

$$E_{perm}\left(RV_{(X,Y)} \right) = \frac{tr(A)tr(B)}{(n-1) \times tr(AA)^{\frac{1}{2}} \times tr(BB)^{\frac{1}{2}}}. \quad (A.2)$$

The variance of permutated $RV(X, Y)$ can be calculated:

$$V_{perm}\left(RV_{(X,Y)} \right) = \frac{2\left((n-1) - \frac{(tr(A))^2}{tr(AA)} \right)\left((n-1) - \frac{(tr(B))^2}{tr(BB)} \right)}{(n-1)^2(n+1)(n-2)}$$

$$+ \frac{\left(n(n+1)\frac{\sum_{i=1}^n \left[x_i^t x_i \right]^2}{tr(AA)} - (n-1)\left(\frac{(tr(A))^2}{tr(AA)} + 2 \right) \right) \cdot \left(n(n+1)\frac{\sum_{i=1}^n \left[y_i^t y_i \right]^2}{tr(BB)} - (n-1)\left(\frac{(tr(B))^2}{tr(BB)} + 2 \right) \right)}{(n+1)n(n-1)(n-2)(n-3)}. \quad (A.3)$$

The mathematical expectation of the log-transformation of the permutated $RV(X, Y)$ is calculated as follows:

$$E_{perm}\left(\log\left(RV_{(X,Y)} \right) \right) = \log\left(E_{perm}\left(RV_{(X,Y)} \right) \right) - \frac{1}{2} \log\left(1 + \frac{V_{perm}\left(RV_{(X,Y)} \right)}{V_{perm}\left(RV_{(X,Y)} \right) + \left(E_{perm}\left(RV_{(X,Y)} \right) \right)^2} \right). \quad (A.4)$$

The variance of the log-transformation of the permutated $RV(X, Y)$:

$$V_{perm}\left(\log\left(RV_{(X,Y)} \right) \right) = \log\left(1 + \frac{V_{perm}\left(RV_{(X,Y)} \right)}{V_{perm}\left(RV_{(X,Y)} \right) + \left(E_{perm}\left(RV_{(X,Y)} \right) \right)^2} \right). \quad (A.5)$$

We obtain a new statistic of standard normal distribution (Formula 13):

$$Z = \frac{\log\left(RV_{(X,Y)} \right) - E_{perm}\left(\log\left(RV_{(X,Y)} \right) \right)}{\sqrt{V_{perm}\left(\log\left(RV_{(X,Y)} \right) \right)}}.$$

The log-transformation of the RV permutation distribution is suggested as a better normal approximation to obtain the real *p*-value without performing actual permutation (Josse et al., 2008).

Appendix B

Many singular value decomposition (SVD)-based multivariate statistical methods, such as PCA (principal component analysis), CCA (canonical correlation analysis), MLM (multivariate linear regression analysis), PLS (Partial least square model analysis) and discriminant analysis can be generalized within the framework of RV-coefficient problem. The following gives the association between the RV coefficient and PCA as well as CCA.

RV coefficient and PCA

Giving $n \times p$ matrix X and $n \times q$ matrix Y, PCA can be interpreted as finding the linear transformation matrix M (M is $q \times r$ matrix with rank r, $q \geq r$), such that for matrix YM, $RV(X, YM)$ are maximized.

Let: $S_{11} = X'X$, $S_{22} = Y'Y$, $S_{12} = X'Y$, $S_{21} = Y'X$

$$\max RV(X, YM) = \max \frac{tr(S_{12}MM'S_{21})}{\sqrt{tr(S_{11}^2)tr(S_{22}^2)}} = \sqrt{\frac{\sum_{i=1}^r \lambda_i^2}{tr(S_{11}^2)}}. \quad (B.1)$$

Eq. (B.1) is obtained when the following constraint-condition is satisfied:

1) $M'S_{22}M = \Lambda$
2) $S_{22}^+ S_{21}S_{12}M = M\Lambda$, S_{22}^+ is pseudoinverse of S_{22}.
3) $\Lambda = diag(\lambda_1, \lambda_2, ... \lambda_r)$ is the eigenvalues of matrix $S_{22}^+ S_{21}S_{12}$, $\lambda_1 \geq \lambda_2 \geq ... \lambda_r$.

Specifically, when $M'M = I_r$,

$$RV(Y, YM) = \sqrt{\frac{\sum_{i=1}^r \lambda_i^2}{\sum_{i=1}^p \lambda_i^2}}. \quad (B.2)$$

More specifically, if $p = r$, which means M is a orthogonal matrix,

$$RV(Y, YM) = 1. \quad (B.3)$$

RV coefficient and CCA

Giving $n \times p$ matrix X and $n \times q$ matrix Y, CCA be interpreted as finding the linear transformation matrix L (L is $p \times r$ matrix with rank r) and M (M is $q \times r$ matrix with rank r) that for matrix XL and YM, $RV(XL, YM)$ are maximized.

Let: $S_{11} = X'X$, $S_{22} = Y'Y$, $S_{12} = X'Y$, $S_{21} = Y'X$

$$\max RV(XL, YM) = \max \frac{tr(L'S_{12}MM'S_{21}L)}{\sqrt{tr(L'S_{11}^2 L)tr(M'SS_{22}^2 M)}} = \frac{\left(\sum_{i=1}^r \gamma_i \delta_{xi} \delta_{yi} \right)}{\sqrt{\sum_{i=1}^r \delta_{xi}^2}\sqrt{\sum_{i=1}^r \delta_{yi}^2}}. \quad (B.4)$$

Eq. (B.4) is obtained when the following constraint-condition is satisfied:

1) $L'S_{11}L = \Delta_x$; $\Delta_x = diag(\delta_{x1}, \delta_{x2}, ... \delta_{xr})$
2) $M'S_{22}M = \Delta_y$; $\Delta_y = diag(\delta_{y1}, \delta_{y2}, ... \delta_{yr})$
3) $S_{11}^+ S_{12}S_{22}^+ S_{21}L = L\Lambda$
4) $S_{22}^+ S_{21}S_{11}^+ S_{12}M = M\Lambda$

where $\Lambda = diag(\gamma_1, \gamma_2, ... \gamma_r)$ is the eigenvalues of matrices $S_{11}^+ S_{12}S_{22}^+ S_{21}$, $S_{22}^+ S_{21}S_{11}^+ S_{12}$, and $\lambda_1 \geq \lambda_2 \geq ... \lambda_r$, S_{11}^+ is pseudoinverse of S_{11}, and S_{22}^+ is pseudoinverse of S_{22}.

Under the above constraint-condition, we can also deduce the following equations:

$$M = S_{22}^{-1} S_{21}L\Lambda^{-\frac{1}{2}}\Delta_x^{-\frac{1}{2}}\Delta_y^{-\frac{1}{2}} \quad (B.5)$$

$$L = S_{11}^{-1} S_{12}M\Lambda^{-\frac{1}{2}}\Delta_y^{-\frac{1}{2}}\Delta_x^{-\frac{1}{2}} \quad (B.6)$$

$$(XL)(YM)' = diag\left(\gamma_1\delta_{x1}\delta_{y1}, \gamma_2\delta_{x2}\delta_{y2}, \dots \gamma_r\delta_{xr}\delta_{yr}\right). \tag{B.7}$$

If we give additional constraint-condition:

5) $(XL)(XL)' = I_r$
6) $(YM)(YM)' = I_r$

where I_r is the identity matrix of size r, the maximum of $RV(XL, YM)$ is equal to:

$$\max RV(XL, YM) = \frac{\left(\sum\limits_{i=1}^{r} \gamma_i\delta_{xi}\delta_{yi}\right)}{r}. \tag{B.8}$$

If we further add constraint-condition: $\delta_{xi} = 1_r$, $\delta_{yi} = 1_r$, $i = 1, 2, \dots r$, the maximum of $RV(XL, YM)$ is

$$RV(XL, YM) = \frac{\sum\limits_{i=1}^{r} \gamma_i}{r}. \tag{B.9}$$

References

Abdi, H., 2007. RV coefficient and congruence coefficient. In: Salkin, Neil (Ed.), Encyclopedia of Measurement and Statistics. Sage, Thousand Oaks (CA), pp. 849–853.

Abdi, H., Valentin, D., O'Toole, A.J., Edelman, B., 2005. DISTATIS: The analysis of multiple distance matrices. Proceedings of the IEEE Computer Society: International Conference on Computer Vision and Pattern Recognition, pp. 42–47 (San Diego, CA, USA).

Abdi, H., Dunlop, J.P., Williams, L.J., 2009. How to compute reliability estimates and display confidence and tolerance intervals for pattern classifiers using the Bootstrap and 3-way multidimensional scaling (DISTATIS). Neuroimage 45, 89–95.

Achard, S., Salvador, R., Whitcher, B., Suckling, J., Bullmore, E., 2006. A resilient, low-frequency, small-world human brain functional network with highly connected association cortical hubs. J. Neurosci. 26, 63–72.

Beckmann, C.F., DeLuca, M., Devlin, J.T., Smith, S.M., 2005. Investigations into resting-state connectivity using independent component analysis. Philos. Trans. R. Soc. Lond. B Biol. Sci. 360, 1001–1013.

Biswal, B., Yetkin, F.Z., Haughton, V.M., Hyde, J.S., 1995. Functional connectivity in the motor cortex of resting human brain using echo-planar MRI. Magn. Reson. Med. 34, 537–541.

Bokde, A.L., Lopez-Bayo, P., Meindl, T., Pechler, S., Born, C., Faltraco, F., Teipel, S.J., Möller, H.J., Hampel, H., 2006. Functional connectivity of the fusiform gyrus during a face-matching task in subjects with mild cognitive impairment. Brain 129, 1113–1124.

Bullmore, E.T., Suckling, J., Overmeyer, S., Rabe-Hesketh, S., Taylor, E., Brammer, M.J., 1999. Global, voxel, cluster tests, by theory and permutation, for a difference between two groups of structural MR images of the brain. IEEE Trans. Med. Imaging 18, 32–42.

Cohen, A.L., Fair, D.A., Dosenbach, N.U., Miezin, F.M., Dierker, D., Van Essen, D.C., Schlaggar, B.L., Petersen, S.E., 2008. Defining functional areas in individual human brains using resting functional connectivity MRI. Neuroimage 41, 45–57.

Cordes, D., Haughton, V.M., Carew, J.D., Arfanakis, K., Maravilla, K., 2002. Hierarchical clustering to measure connectivity in fMRI resting-state data. Magn. Reson. Imaging 20, 305–317.

Damoiseaux, J.S., Rombouts, S.A., Barkhof, F., Scheltens, P., Stam, C.J., Smith, S.M., Beckmann, C.F., 2006. Consistent resting-state networks across healthy subjects. Proc. Natl Acad. Sci. USA 103, 13848–13853.

Escoufier, Y., 1973. On vector random variables (French: Le traitement des variables vectorielles). Biometrics 29, 751–760.

Fox, M.D., Snyder, A.Z., Vincent, J.L., Corbetta, M., Van Essen, D.C., Raichle, M.E., 2005. The human brain is intrinsically organized into dynamic, anticorrelated functional networks. Proc. Natl Acad. Sci. USA 102, 9673–9678.

Friman, O., Borga, M., Lundberg, P., Knutsson, H., 2003. Adaptive analysis of fMRI data. Neuroimage 19 (3), 837–845.

Gitelman, D.R., Penny, W.D., Ashburner, J., Friston, K.J., 2003. Modeling regional and psychophysiologic interactions in fMRI: the importance of hemodynamic deconvolution. Neuroimage 19, 200–207.

Greicius, M.D., Krasnow, B., Reiss, A.L., Menon, V., 2003. Functional connectivity in the resting brain: a network analysis of the default mode hypothesis. Proc. Natl Acad. Sci. 100, 253–258.

Hamani, El.Maâche., Yves, Lepage., 2007. Tests for assessing vector correlation. Model Assist. Stat. Appl. 2, 3–15.

Hampson, M., Peterson, B.S., Skudlarski, P., Gatenby, J.C., Gore, J.C., 2002. Detection of functional connectivity using temporal correlations in MR images. Hum. Brain Mapp. 15, 247–262.

Harrison, L., Penny, W.D., Friston, K.J., 2003. Multivariate autoregressive modeling of fMRI time series. Neuroimage 19, 1477–1491.

Hayasaka, S., Nichols, T.E., 2004. Combining voxel intensity and cluster extent with permutation test framework. Neuroimage 23, 54–63.

Heo, M., Gabriel, K.R., 1998. A permutation test of association between configurations by means of the RV coefficient. Comm. Stat. Simulat. Comput. 27 (3), 843–856.

Jiang, T.Z., He, Y., Zang, Y.F., Weng, X.C., 2004. Modulation of functional connectivity during the resting state and the motor task. Hum. Brain Mapp. 22 (1), 63–71.

Josse, J., Husson, F., Pages, J., 2008. Testing the significance of the RV coefficient. Comput. Statist. Data Anal. 53, 82–91.

Kazi-Aoual, Frederique, Hitier, Simon, Sabatier, Robert, Lebreton, Jean-Dominique, 1995. Refined approximations to permutation tests for multivariate inference. Comput. Statist. Data Anal. 20, 643–656.

Kherif, F., Poline, J.B., Mériaux, S., Benali, H., Flandin, G., Brett, M., 2003. Group analysis in functional neuroimaging: selecting subjects using similarity measures. Neuroimage 20, 2197–2208.

Kriegeskorte, N., Goebel, R., Bandettini, P., 2006. Information-based functional brain mapping. Proc. Natl Acad. Sci. USA 103, 3863–3868.

Kubinger, K.D., Rasch, D., Šimeckova, M., 2007. Testing a correlation coefficient's significance: using $H_0: 0 < \rho \leq \lambda$ is preferable to $H_0: \rho = 0$. Psychol. Sci. 49, 74–87.

Lowe, M.J., Mock, B.J., Sorenson, J.A., 1998. Functional connectivity in single and multislice echoplanar imaging using resting state fluctuations. Neuroimage 7, 119–132.

Mardia, K.V., 1971. The effect of nonnormality on some multivariate tests and robustness to nonnormality in the linear model. Biometrika 58 (1), 105–121.

Margulies, D.S., Kelly, A.M., Uddin, L.Q., Biswal, B.B., Castellanos, F.X., Milham, M.P., 2007. Mapping the functional connectivity of anterior cingulate cortex. Neuroimage 37, 579–588.

Maxim, V., Sendur, L., Fadili, J., Suckling, J., Gould, R., Howard, R., Bullmore, E., 2005. Fractional Gaussian noise, functional MRI and Alzheimer's disease. Neuroimage 25, 141–158.

McIntosh, A.R., Chau, W.K., Protzner, A.B., 2004. Spatiotemporal analysis of event-related fMRI data using partial least squares. Neuroimage 23, 764–775.

Mielke, P.W., 1978. Clarification and appropriate inferences for Mantel and Valand's nonparametric multivariate analysis technique. Biometrics 34, 277–282.

Mielke, P.W., 1979. On asymptotic non-normality of null distributions of MRPP statistics. Commun. Stat. Theory Meth. 8, 1541–1550.

Nandy, R., Cordes, D., 2004. Improving the spatial specificity of canonical correlation analysis in fMRI. Magn. Reson. Med. 52, 947–952.

Nir, Y., Hasson, U., Levy, I., Yeshurun, Y., Malach, R., 2006. Widespread functional connectivity and fMRI fluctuations in human visual cortex in the absence of visual stimulation. Neuroimage 30, 1313–1324.

Poline, J.B., Worsley, K.J., Evans, A.C., Friston, K.J., 1997. Combining spatial extent and peak intensity to test for activations in functional imaging. Neuroimage 5, 83–96.

Ragnehed, M., Engström, M., Knutsson, H., Söderfeldt, B., Lundberg, P., 2009. Restricted canonical correlation analysis in functional MRI-validation and a novel thresholding technique. J. Magn. Reson. Imaging 29, 146–154.

Robert, P., Escoufier, Y., 1976. A unifying tool for linear multivariate statistical methods: the RV coefficient. Appl. Stat. 25, 257–265.

Robinson, S., Basso, G., Soldati, N., Sailer, U., Jovicich, J., Bruzzone, L., Kryspin-Exner, I., Bauer, H., Moser, E., 2009. A resting state network in the motor control circuit of the basal ganglia. BMC Neurosci. 23, 10–137.

Rydell, J., Knutsson, H., Borga, M., 2006. Adaptive filtering of fMRI data based on correlation and bold response similarity. IEEE International Conference on Acoustics, Speech and Signal Processing, Toulouse, France.

Salvador, R., Suckling, J., Coleman, M.R., Pickard, J.D., Menon, D., Bullmore, E., 2005. Neurophysiological architecture of functional magnetic resonance images of human brain. Cereb. Cortex 15, 1332–1342.

Shinkareva, S.V., Ombao, H.C., Sutton, B.P., Mohanty, A., Miller, G.A., 2006. Classification of functional brain images with a spatio-temporal dissimilarity map. Neuroimage 33, 63–71.

Terumitsu, M., Ikeda, K., Kwee, I.L., Nakada, T., 2009. Participation of primary motor cortex area 4a in complex sensory processing: 3.0-T fMRI study. NeuroReport 20 (7), 679–683.

Tomasi, C., Manduchi, R., 1998. Bilateral filtering for Gray and Color Images. IEEE International Conference on Computer Vision, Bombay, India.

Xiong, J., Parsons, L.M., Gao, J.H., Fox, P.T., 1999. Interregional connectivity to primary motor cortex revealed using MRI resting state images. Hum. Brain Mapp. 8, 151–156.

Zang, Y.F., Jiang, T.Z., Lu, Y.L., He, Y., Tian, L.X., 2004. Regional homogeneity approach to fMRI data analysis. Neuroimage 22, 394–400.